APS physics

CHORUS

This is the accepted manuscript made available via CHORUS. The article has been published as:

Design of a polar half-metallic ferromagnet with accessible and enhanced electric polarization

Danilo Puggioni, Alessandro Stroppa, and James M. Rondinelli

Phys. Rev. Materials **2**, 114403 — Published 12 November 2018

DOI: 10.1103/PhysRevMaterials.2.114403

Design of a polar half-metallic ferromagnet with accessible and enhanced electric polarization

Danilo Puggioni,[1] Alessandro Stroppa,[2] and James M. Rondinelli[1]

[1] *Department of Materials Science and Engineering, Northwestern University, Evanston, Illinois 60208, USA*
[2] *CNR-SPIN L'Aquila, Via Vetoio 10, I-67100 L'Aquila, Italy*

We design a compound belonging to a new class of materials designated as polar half-metallic ferromagnets (pHMFs), where a 100% spin polarization coexists with polar distortions that globally lift inversion symmetry. Using electronic structure calculations, we predict that the ultrashort period $(LaNiO_3)_1/(YCrO_3)_1$ superlattice belongs to this materials class, exhibiting an integer magnetic moment of 4 μ_B. The minority channel polarization, as computed using Berry phase theory, is as high as $\sim 13.0\,\mu C\,cm^{-2}$, and we discuss experimental strategies to access the polarization. We propose that polar ferromagnetic half-metals exhibit multiferroism and can be exploited to realize non-reciprocal effects and directional anisotropy owing to the absence of both space-inversion and time-reversal symmetries.

I. INTRODUCTION

Band conductors with unusual electronic or atomic structures offer a materials platform from which to access novel functionalities. Half-metallic ferromagnets (HMF) with their unique band structures were introduced more than thirty years ago on the basis of electronic structure calculations performed on PtMnSb and NiMnSb.[1] The electrons in one spin channel occupy a partially filled band, manifesting as a well-defined Fermi surface; however, the opposite spin channel is gapped, leading to insulating behavior. These compounds exhibit responses to electric and magnetic fields that differ from those expected for simple band metals upon cooling toward zero kelvin. For example, although there is electrical conductivity with a spin-polarized current, the magnetic susceptibility vanishes because of the spin-flip gap.[2] This does not occur in simple or binary transition metal ferromagnets, which exhibit a nearly filled majority spin nd-derived band intersecting a free-electron $(n+1)s$ band with spins from both spin channels.[3] All HMFs contain multiple transition metals and frequently exhibit the Heusler structure-type[1,4] or are found among ternary or quaternary oxides with perovskite-derived structures.[5,6] Owing to these properties, HMF materials continue to be of both fundamental interest, as they can support topological fermions,[7] and enable numerous magnetoresistance and spintronic technologies.[8]

Another intriguing class of band conductors are those classified as polar metals (PMs). Although these materials were partially conceptualized more than 50 years ago,[9] they are of renewed interest owing to the synthesis and characterization of $LiOsO_3$ (Ref. 10) and $Ca_3Ru_2O_7$ (Ref. 11). This osmate exhibits the polar $R3c$ lithium-niobate structure and Fermi liquid-like transport[10] whereas the layered perovskite ruthenate exhibits a complex temperature dependent phase diagram.[12] The theoretical appeal of PMs lies in the coexistence of perceived incompatible features—polar distortions and metallicity. In a metal, free electrons screen the long-range electrostatic forces that favor a polar structure. Thus, it is surprising to find metals that exhibit parity-lifting displacive transitions. Nonetheless, often this incompatibility in PMs is overcome because the polar distortions are largely decoupled from the charge carriers at the Fermi level responsible for electrical conductivity.[13] In contrast to HMFs, only a small number of PMs are oxides.[13,14] Although PMs are not ferroelectrics, in the sense that there is a well-defined and reversable electric polarization, the materials offer a platform for studying unusual phenomena such as magnetoelectricity,[15] exotic superconductivity,[16] and unconventional optical responses.[17]

Here we propose a design strategy to realize polar half-metals ferromagnets (pHMFs) – materials where half-metallicity coexists with polar distortions – for which at present we are unaware of any examples. The pHMFs exhibit metallic spin-polarized currents owing to a fully gapped spin channel and show long-range ferromagnetic order, which makes them a subclass of materials arising from the intersection of the broader classes of noncentrosymmetric metals and half-metallic ferromagnets. Our design strategy exploits cation ordering to achieve a half-metallic electronic structure and polar displacements induced by multimode lattice interactions. We demonstrate with first-principles density functional theory (DFT) how the ultrashort period $(LaNiO_3)_1/(YCrO_3)_1$ superlattice fulfills our design criteria, making it the first oxide member of this materials family. The ground state exhibits a polar monoclinic Pb crystal structure with integer magnetization, 4 μ_B. We also compute the electric polarization of the minority (insulating) spin channel, which amounts to about 13.0 $\mu C\,cm^{-2}$ and should persist above room temperature. Last, we propose that an external electric field can be used to switch the electronic polarization of the minority-spin channel.

II. METHODS AND MATERIALS

We perform first-principles DFT calculations within the Perdew-Burke-Ernzerhof (PBE)[18] generalized gradient approximation as implemented in the Vienna *Ab initio* Simulation Package (VASP)[19] with the projector augmented wave (PAW) approach[20] to treat the core and valence electrons using the following electronic configurations $5s^25p^65d^16s^2$ (La), $4s^24p^64d^15s^2$ (Y), $3d^84s^2$ (Ni), $3d^54s^1$ (Cr), $2s^22p^4$ (O) with a $7\times7\times5$ Monkhorst-Pack k-point mesh[21] and a 600 eV planewave cutoff. Electronic correlation effects among the transition metal $3d$ orbitals are considered by using a single effective Hubbard parameter, $U_{\text{eff}} = U - J$, hereafter referred to as U following Ref. 22. Different U values, ranging from 1 to 7 eV, are used for both the Cr and Ni cations.

We simulate all $(LaNiO_3)_1/(YCrO_3)_1$ structures by imposing a biaxial mechanical constraint such that the in-plane lattice constants are equal to simulate thin-film growth of an oxide superlattice on substrate with a square lattice net. All interaxial unit cell angles are constrained to 90°. Note that $YCrO_3$ (Ref. 23) and $LaNiO_3$ (Ref. 24) have a lattice mismatch of ∼1.3%, suggesting that ultrashort period superlattices are experimentally feasible. Furthermore, the recent developments in the growth of perovskite oxides superlattices make it possible to deposit smooth films layer-by-layer with high quality.[25] However, we note that from the experimental point of view, it could be challenging to obtain the [001] layered ordering of B/B′ cations in $A_2BB'O_6$ perovskites.[26]

We search for ground state crystal structures by using the frozen-phonon method[27,28] to calculate the phonon frequencies and eigendisplacements of the ultrashort-period $(LaNiO_3)_1/(YCrO_3)_1$ superlattice where the A-site (La and Y) and B-site (Ni and Cr) cations are both ordered along the [001] direction (space group $P4mm$). Next, we systematically 'freeze-in' linear combinations of the unstable modes into this reference phase, performing structural optimization on the generated lower symmetry polymorphs until obtaining the global minimum. For all calculations, we relax the atomic positions (forces <0.1 meV Å^{-1}) using Gaussian smearing (20 meV width). The group theoretical analyses are performed with the AMPLIMODES software.[29,30]

III. RESULTS AND DISCUSSION

A. Design Strategy

Double perovskites with composition $A_2BB'O_6$, such as La_2NiMnO_6 (Ni^{2+}/Mn^{4+}), La_2NiCrO_6 (Ni^{2+}/Cr^{4+}), and La_2CoMnO_6 (Co^{2+}/Mn^{4+}) exhibit an ordered rock-salt arrangement of B-site cations, i.e., [111]-ordering direction of corner-sharing BO_6 and $B'O_6$ units,[31–33] and are ferromagnetic insulators. The magnetic ordering is due to the rock-salt arrangement of the B-site cations which favors the ferromagnetic interaction in the 180° B(t_{2g})–O–B′(e_g) linear chain according to the Goodenough-Kanamori rules.[34–36] The insulating states in La_2NiCrO_6 ($t_{2g}^6e_g^2/t_{2g}^2e_g^0$) and La_2CoMnO_6 ($t_{2g}^5e_g^2/t_{2g}^3e_g^0$) are driven by Coulomb correlation and Coulomb-assisted spin-orbit coupling, respectively.[33,37] Differently, in La_2NiMnO_6 the insulating state derives from the half filling of the $3d$ orbitals ($t_{2g}^6e_g^2/t_{2g}^3e_g^0$);[38] nonetheless, electronic correlations are crucial for a complete description of the electrical properties.[32]

TABLE I. Design strategy for a perovskite-structured polar half-metallic ferromagnet (pHMFs) exhibiting the $a^-a^-c^+$ tilt pattern. The ✓and × indicate whether a given criteria is satisfied or not, respectively, by the A or B site chemical order (first column).

A-Site Ordering	Half-metallic ferromagnet	Polar symmetry
[001]	×	✓
[110]	×	×
B-Site Order		
[001]	✓	×
[110]	✓	×
A- and B-Site Order		
[001] and [001]	✓	✓
[001] and [110]	✓	✓
[110] and [100]	✓	×
[110] and [110]	✓	×

When the B-site chemical order switches from [111] to a [001] or [110] arrangement, these compounds transform into half-metallic ferromagnets (HMFs).[32,33] They also exhibit the $a^-a^-c^+$ tilt pattern in Glazer notation;[39] therefore, spatial inversion symmetry can be broken by combining B-site order with A-site order owing to multimode lattice interactions.[40] Although the combination of mixed-rotation patterns and A-site ordering along the [110]-direction is not a useful route to produce polar compounds, A-cation order along the [001] direction with such octahedral rotation patterns may result in a perovskite without inversion symmetry owing to anti-polar A-site displacements that do not fully cancel.[41] In addition, the polar displacements that derive from the A-site cations in perovskites typically do not contribute to the electronic structure at the Fermi level, which is also in agreement with a polar metal design strategy introduced by two of us.[13]

The combination of all these ingredients (Table I) naturally suggests two possible strategies to realize polar HMFs: i) layered cation ordering for both the A- and B- cations and ii) layered ordering of the A-cations with [110] ordering of the B-cations. Here we follow the first strategy and therefore we analyze the crystal structure and electronic properties of the $(LaNiO_3)_1/(YCrO_3)_1$ superlattice exhibiting [001] cation ordering for both the A- and B- cations. The results concerning the combination

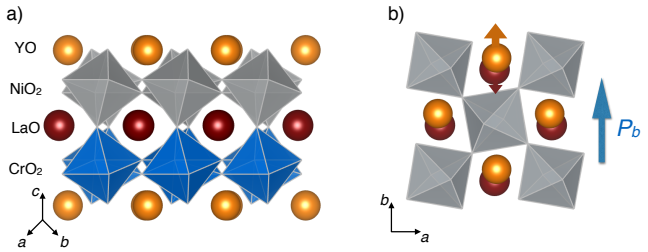

FIG. 1. Polar monoclinic crystal structure, Pb symmetry, of $(LaNiO_3)_1/(YCrO_3)_1$ with the $a^-b^-c^+$ tilt pattern. (a) The La and Y cations (A sites) and Ni and Cr cations (B-sites) are ordered along the [001] direction. (b) The direction of the dipolar order arises from the La and Y displacements (small cation-centered arrows) that do not compensate along the [010] direction.

of [001] ordering of the A-cations with [110] ordering of the B-cations will be presented elsewhere.

B. Crystal Symmetry and Dynamical Stability

Fig. 1 depicts the polar Pb ground state crystal structure of $(LaNiO_3)_1/(YCrO_3)_1$ obtained from DFT-PBE (Table II). The NiO_6 and CrO_6 octahedra are highly rotated, exhibiting the $a^-b^-c^+$ tilt system as anticipated for low tolerance factor perovskites. Here, the in-phase octahedral rotation axis c^+ corresponds to the film's normal (growth) direction. The Cr–O–Ni bond angles perpendicular to the LaO/YO monoxide layers are 155.1° and 144.8°, whereas the average Ni-O–Ni and Cr–O–Cr bond angles are 153.5° and 151.7°, respectively.

The polar displacements in $(LaNiO_3)_1/(YCrO_3)_1$ originate from the ordering of the A- and B-cations along the [001] direction (Fig. 1a) and from the antiparallel and uncompensated displacements along the [010] direction of the A-cations (Fig. 1b). We point out that the layered ordering of the the A- and B- cations naturally breaks the inversion symmetry along the [001] direction of the $(LaNiO_3)_1/(YCrO_3)_1$ superlattice resulting in the polar space group $P4mm$. Therefore, the polarization along the [001] direction is nonzero, however regardless of the electronic properties of the material, it is not switchable because it originates from the chemical ordering. For this reason we focus on the switchable in-plane component. The polar displacements of La and Y atoms with respect the $P4mm$ phase along the [010] direction are -0.23 Å and 0.34 Å, respectively. For a dielectric, these polar displacements would result in a net electric dipole oriented along the b axis, P_b, as shown in Fig. 1b. Note that intermediate polymorphs with $a^0a^0c^+$ and $a^-a^-c^0$ (as well as $a^0a^0c^0$) tilt patterns are higher in energy consistent with reports on hybrid improper ferrolectrics.[42] Moreover, we find small acentric B-sites (Ni and Cr) displacements (<0.02 Å) along the [100] direction.

Using symmetry mode analysis,[29,30] we decompose the ground state Pb structure into a set of symmetry-adapted modes associated with different irreducible representations (irreps) of the $P4mm$ phase. Recall that $P4mm$ exhibits with the same cation order, but octahedral rotations and polar displacements, along the [010] direction, are absent. We find that all of the aforementioned displacements are described by three main symmetry modes that transform as irreps Γ_5, M_2, and M_5 of $P4mm$. The modes Γ_5 at $k = (0,0,0)$ and M_2 and M_5 at $k = (1/2,1/2,0)$ correspond to the polar ir-active mode along the [010] direction and the in-phase and out-of-phase octahedral rotation modes, respectively. Owing to the symmetry of these modes, our analysis indicates the octahedral rotations couple together to drive the $P4mm \rightarrow Pb$ symmetry reduction, and therefore the in-plane polar displacements arise through an anharmonic interaction that is also active to support hybrid-improper ferroelectricity.[43]

TABLE II. Crystallographic parameters for monoclinic $(LaNiO_3)_1/(YCrO_3)_1$ calculated within PBE. Electronic correlations slightly affect the structural parameters by less than 3 %. Although the cell remains metrically tetragonal ($\alpha = \beta = \gamma = 90°$), the internal degrees of freedom reduce the symmetry to monoclinic.

Pb (Space group no. 7)		$a = b = 5.4994$ Å, $c = 7.4746$ Å		
Atom	Wyck. Site	x	y	z
La	2a	0.25550	0.95655	0.00856
Y	2a	0.23737	0.06031	0.49298
Ni	2a	0.25303	0.50071	0.25580
Cr	2a	0.25256	0.50291	0.74319
O(1)	2a	0.17638	0.50944	0.99830
O(2)	2a	0.54700	0.70352	0.78618
O(3)	2a	0.95618	0.29276	0.69443
O(4)	2a	0.54343	0.70578	0.21829
O(5)	2a	0.96063	0.28976	0.30384
O(6)	2a	0.35241	0.46877	0.50107

C. Electronic Properties

Fig. 2 shows the electronic density-of-states (DOS) for $(LaNiO_3)_1/(YCrO_3)_1$ without correlation effects [$U(\mathrm{Ni,Cr}) = 0\,\mathrm{eV}$] (see Ref. 44 for the electronic band structure). We find the although the superlattice is metallic, it is near a metal-to-half-metal transition owing to the pseudogap appearing at 1 eV below the Fermi level, E_F, in the minority spin derived Ni states. In the spin-up channel, the E_F is dominated by the Cr-derived t_{2g} states with a smaller contribution from the e_g states of the Ni atom. The Ni t_{2g} states are mainly localized from -2 to -1 eV below E_F. Moreover, the Cr and Ni 3d states are strongly hybridized with the oxygen 2p-states, indicating the presence of covalent Cr–O and Ni–O bonds throughout the superlattice. In addition, the La and Y

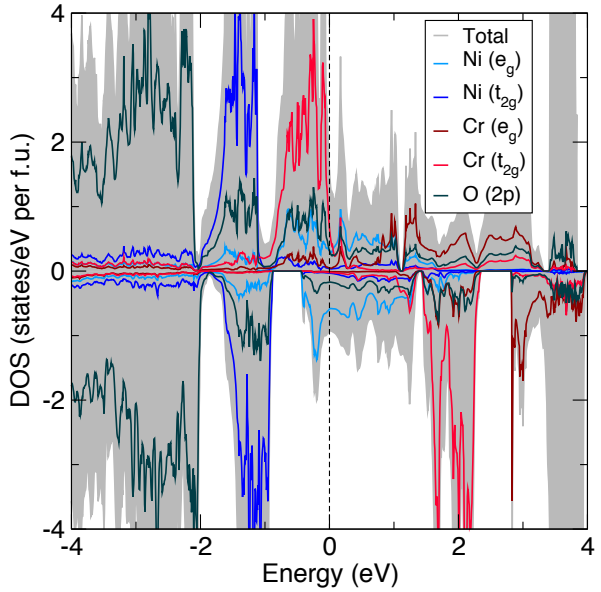

FIG. 2. The atom- and orbital-projected density of states (DOS) for $(LaNiO_3)_1/(YCrO_3)_1$ calculated within DFT-PBE. The Fermi level is at 0 eV (broken vertical line).

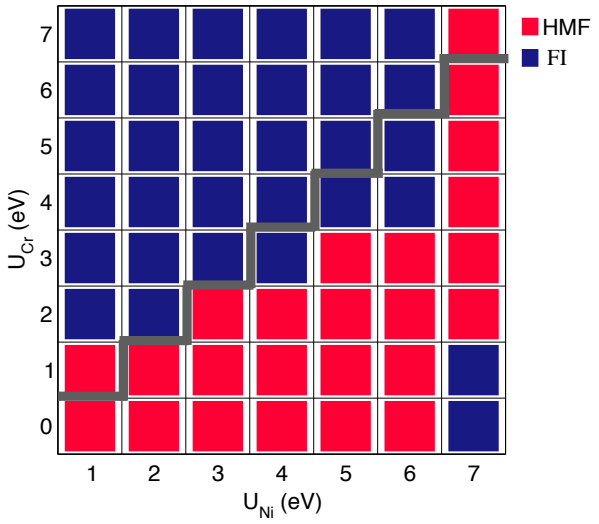

FIG. 3. Electronic and magnetic phase diagram of $(LaNiO_3)_1/(YCrO_3)_1$ as a function of the degree of electronic correlation among the Ni and Cr $3d$ orbitals. Red and blue squares indicate the ferromagnetic insulating (FI) and half-metallic ferromagnetic (HMF) phase, respectively. All states lack inversion symmetry. The gray line divides the phase diagram in two regions where $U_{\rm Cr} \geq U_{\rm Ni}$ and $U_{\rm Cr} < U_{\rm Ni}$.

states are located far from the Fermi level, which justifies the stability of the metallic polar state through the weak electron-lattice coupling principle.[13] The incompatibility between polar distortions and metallicity is circumvented because the inversion-lifting distortions arise from ions which have minor orbital contributions to the low-energy electronic structure.

We find that the $(LaNiO_3)_1/(YCrO_3)_1$ superlattice exhibits ferromagnetic (FM) spin order at the DFT-PBE level, and this spin configuration is $\sim$6.0 meV f.u.$^{-1}$ more stable than a ferrimagnetic metallic phase, whereby the local magnetic moments on Ni and Cr are anti-aligned. Specifically, the total magnetic moment is nearly integer (approximately 3.0 μ_B f.u.$^{-1}$) due to local moments of $\sim$0.2 μ_B and $\sim$2.6 μ_B on the Ni and Cr cations, respectively. The value of the local magnetic moments are consistent with low-spin Ni^{3+} ($S = 1/2$) and Cr^{3+} ($S = 3/2$) configurations. The remaining magnetization is distributed among the oxide anions forming the corner-connected octahedral network due to the itinerant spin-polarized electrons. Note that the local moment of Ni^{3+} is considerably reduced due to strong $pd\sigma$ bonding interactions.

D. Correlation Effects

A more accurate theoretical description of the electronic state of $3d$ transition metal oxides often requires that static (or dynamical) electronic correlations are accounted for within a band-theory approach. For example, the local spin-density approximation finds that $NiCrO_3$ is a compensated half-metal;[45] however, a nonzero onsite Coulomb interaction for Ni and Cr is needed to obtain a semiconducting $NiCrO_3$ in agreement with experimental transport measurements.[46]

The DOS of $(LaNiO_3)_1/(YCrO_3)_1$ at the DFT-PBE level shows that the e_g (t_{2g}) states of Ni (Cr) atoms are strongly localized, with a bandwidth of $\sim$ 2 eV at the Fermi level (Fig. 2). Therefore, it is expected that correlation effects play an important role in the description of the electronic properties of the superlattice. At the same time, correlation effects weakly affect the noncentrosymmetric state in polar metals owing to the weak-coupling principle.[13] For these reasons, we examine the evolution in the electronic state of $(LaNiO_3)_1/(YCrO_3)_1$ with respect to correlation strength within the polar Pb symmetry and emphasize that the experimental superlattice should have $U_{\rm Cr} \neq U_{\rm Ni} \neq 0$ values.

Fig. 3 shows the electronic phase diagram of $(LaNiO_3)_1/(YCrO_3)_1$ with the polar Pb crystal structure as a function of electronic correlation strength within the $3d$ manifolds of Ni and Cr. For each value of U the crystal structure is fully relaxed. For all $U \neq 0$ values, we find the FM state is favored with respect to the ferrimagnetic phase and the net magnetization is both integer, 4.0 μ_B f.u.$^{-1}$ indicating the opening of a gap in the electronic structure, and its value is independent of the interaction strength. As expected the electronic correlations increase the local Ni and Cr magnetic moments such that they range from $\sim$1.2 μ_B to $\sim$1.5 μ_B and from $\sim$2.4 μ_B to $\sim$3.1 μ_B, respectively. As in the uncorrelated $(LaNiO_3)_1/(YCrO_3)_1$ structure, the remaining magnetization is distributed among the oxygen atoms.

The occupied (unoccupied) states shift to higher (lower)

energy as the degree of electronic correlation increases within the correlated Ni and Cr $3d$ manifold. As a result, the superlattice is no longer metallic (as in the $U = 0$ limit) and transforms to either a half-metal (with a minority spin gap) or an insulator (with both spin channels gap). In addition, an insulator-to-half-metal transition occurs as the correlation strength evolves; therefore, the phase diagram presented in Fig. 3 essentially consists of two main regions. The first region is defined for $U_{\rm Cr} \geq U_{\rm Ni}$. Here $(LaNiO_3)_1/(YCrO_3)_1$ is insulating with a band gap which ranges between 40 meV between the spin-up and spin-down channels ($U_{\rm Cr} = 2\,$eV, $U_{\rm Ni} = 1\,$eV) and 125 meV in the spin-up channel ($U_{\rm Cr} = 7\,$eV, $U_{\rm Ni} = 6\,$eV). The second region is given by $U_{\rm Cr} < U_{\rm Ni}$, and a HMF state is stable with a band gap in the minority-spin channel ranging from $\sim$1.0 eV (for $U_{\rm Cr} = 0\,$eV, $U_{\rm Ni} = 1\,$eV) and $\sim$3.2 eV ($U_{\rm Cr} = 6\,$eV, $U_{\rm Ni} = 7\,$eV).

Although we do not know the exact U values to describe $(LaNiO_3)_1/(YCrO_3)_1$, we propose that the relevant correlation-strength range is limited to $U_{\rm Cr} < U_{\rm Ni}$, because Ni follows Cr in the $3d$ transition metal row. In addition, previous theoretical studies based on DFT+U methods report U values of 6 to 8 eV for Ni (Ref. 47) and 4 to 8 eV for Cr (Ref. 48) for electronically and structurally similar oxides. Therefore, we focus our remaining analysis of $(LaNiO_3)_1/(YCrO_3)_1$ to two scenarios, such that $U_{\rm Cr}$ =5 eV and $U_{\rm Ni} = 6$ or 7 eV. Note that structures for (U_{Cr} =5 eV, U_{Ni} =7 eV) and (U_{Cr} =5 eV, U_{Ni} =6 eV) are reported in the Supporting Information.[44] In addition, the inclusion of spin-orbit interactions do not affect the band structure as shown in Ref. 44. We emphasize that our results for $(LaNiO_3)_1/(YCrO_3)_1$ do not depend on the possible physical choices of correlation-strength ($U_{\rm Cr} < U_{\rm Ni}$) as the pHMF turns out to be the more favorable solution.

Fig. 4(a) shows the DOS of $(LaNiO_3)_1/(YCrO_3)_1$ with $U_{\rm Cr} = 5\,$eV and $U_{\rm Ni} = 7\,$eV (see Ref. 44 for the electronic band structure). With this degree of electronic correlations, we find the superlattice is ferromagnetic, making it a pHMF that is 80 meV f.u.$^{-1}$ more stable than a half-metallic phase with anti-aligned Ni and Cr local magnetic moments. The half-metallicity arises from the $\sim$3.2 eV gap between the O ($2p$) and Ni ($3d$ e_g) states in the minority spin channel due to the electronic correlations. The spin-gap results in a $4\,\mu_B$ f.u.$^{-1}$ magnetization with an enhanced local magnetic moment of $\sim 1.5\,\mu_B$ and $\sim 3\,\mu_B$ on the Ni and Cr ions, respectively, relative to the uncorrelated $U = 0$ case. Interestingly, the net manetization of $4\,\mu_B$ f.u.$^{-1}$ is due to the coordinating oxygen sites which have local magnetic moments that are antiferromagnetically coupled with the Ni and Cr atoms. Note that this mechanism does not depend on the electron correlation strength. In other words, the net magnetization of $(LaNiO_3)_1/(YCrO_3)_1$ is always $4\,\mu_B$ f.u.$^{-1}$ independent of the value of U used in our calculations. In the majority spin channel, we find a pseudogap opens at E_F, with the strongest contribution from oxygen $2p$ states. Moreover, throughout the entire valence band the t_{2g}^3- and e_g^1-states

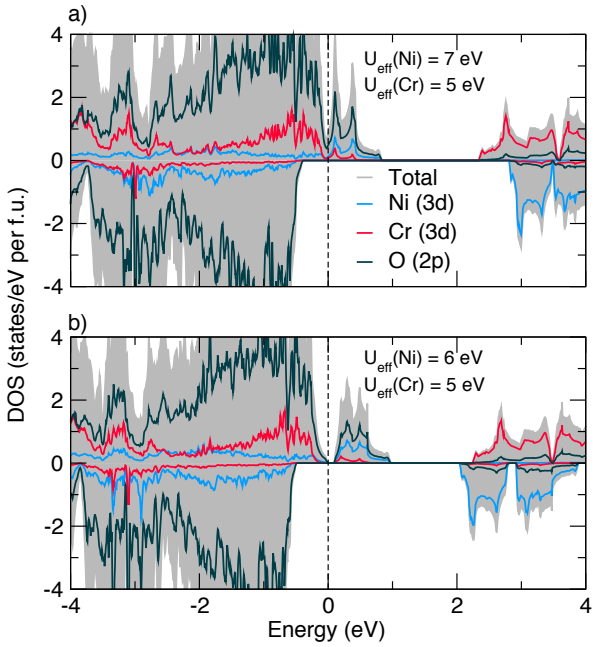

FIG. 4. Electronic DOS of $(LaNiO_3)_1/(YCrO_3)_1$ with (a) $U_{\rm Cr} = 5\,$eV and $U_{\rm Ni}$ =7 eV and (b) $U_{\rm Cr} = 5\,$eV and $U_{\rm Ni} = 6\,$eV. Although $(LaNiO_3)_1/(YCrO_3)_1$ is a polar half-metallic ferromagnet (pHMF) in (a), in transforms to a polar ferromagnetic insulator (pFI) in (b) with a 84 meV gap opening in the majority-spin channel resulting in a multiferroic state.

of Cr and Ni, respectively, exhibit strong O $2p$ admixture.

Upon decreasing the correlation strength within the Ni $3d$ orbitals from $U_{\rm Ni} = 7\,$eV to 6 eV, we find that the pseudogap opens, forming an insulating majority spin channel [Fig. 4(b) and Ref. 44] and $(LaNiO_3)_1/(YCrO_3)_1$ transforms into a polar ferromagnetic insulator (FI). The polar FI state is 49 meV f.u.$^{-1}$ more stable than the ferrimagnetic insulating phase. As expected, the gap in the minority-spin channel is reduced ($\sim$2.50 eV) because of the decrease in electronic correlation strength which shifts the Ni states to higher energy. In addition, the magnetic moment of the Ni cations is slightly reduced to $\sim 1.3\,\mu_B$; however, because of the insulating channel, an integer magnetization must be maintained and this is accomplished by a change in the local moment on the oxide anions; the value of the compensating O $2p$ moment decreases. It is interesting to note that this compensating mechanism is always active independent of the electronic correlation strength. If the local magnetic moment on the Ni (Cr) increases/decreases then the local magnetic on the Cr (Ni) cations decreases (increases). In this complex feedback,[49] the oxygen anions are fundamental in regulating the net integer magnetization, which is a requirement for achieving 100% spin polarized currents. Assessment of the spin Hall conductivity would be a useful tool to examine this feature.[50]

E. Electric Polarization

Owing to the presence of the insulating channel in the *p*HMF phase, we next evaluate the electric polarization using the Berry phase approach[51] for $(LaNiO_3)_1/(YCrO_3)_1$ given in [Fig. 4(a)]. The spontaneous electric polarization is 13.0 μCcm^{-2} along the [010]-direction, defined as P_b in Fig. 1(b). Next, we calculate the spontaneous electric polarization in the *p*FI phase, Fig. 4(b) and find $P_b = 7.1\ \mu C\,cm^{-2}$. Interestingly, the fully insulating phase has lower polarization than the half-metallic state. While only the spin-down channel contributes to the 'ferroelectric polarization' in the *p*HMF case, both spin channels contribute to the electronic polarization of the ferromagnetic insulating case. Thus, the sum of the electronic and the ionic contribution is closer to the polarization quantum in the *p*FI phase than in the *p*HMF phase, which explains the enhanced polarization in the *p*HMF. Now, one can ask if the electronic polarization in the *p*HMF case can be switched under the application of an external electric field. Our assessment indicates the answer is yes. Although the majority-spin charges will screen the electric field, the minority-spin charges will respond as bound electrons as in a dielectric,[52] making the *p*HMF a true multiferroic.

IV. CONCLUSIONS

We proposed a subclass of polar metals with experimentally accessible electric polarizations where half-metallicity coexists with polar distortions. We show that cation ordering is a useful strategy to design half-metallicity and lift inversion symmetry as demonstrated in the $(LaNiO_3)_1/(YCrO_3)_1$ superlattice with [001]-chemical order. Our results suggest that if this cation order sequence is maintained, then other possible polar half-metallic ferromagnets (*p*HMFs) could be found in $(LaNiO_3)_1/(YMnO_3)_1$ and $(LaCoO_3)_1/(YMnO_3)_1$ superlattices. We hope this work motivates the synthesis of *p*HMFs, and provides new materials platforms for accessing non-linear and non-reciprocal effects and complex spin textures, including directional dichroism, magnetochiral anisotropy, and skyrmion states. For example, it recently has been proposed that the magneto-optical Kerr effect could be tuned both by using magnetic degrees of freedom and the electric polarization through the electric-magneto-optical Kerr effect (EMOKE).[53] Here, we speculate that the Kerr spectra could be tuned by the polar distortions thus giving a signature of different polar states. Alternatively, non-reciprocal charge transport[54] could manifest in the magnetotransport measurements on *p*HMFs.

ACKNOWLEDGMENTS

D.P. and J.M.R. acknowledge the ARO under Grant No. W911NF-15-1-0017 for financial support and the DOD-HPCMP for computational resources. A.S. thanks W. Ren for his hospitality at Shanghai University through the Eastern Scholar Program from the Shanghai Municipal Education Commission.

[1] R. A. de Groot, F. M. Mueller, P. G. v. Engen, and K. H. J. Buschow, Phys. Rev. Lett. **50**, 2024 (1983).
[2] H. Eschrig and W. Pickett, Solid State Communications **118**, 123 (2001).
[3] M. Jhonson, *Magnetoelectronics* (Oxford University Press, 1985).
[4] K. Inomata, S. Okamura, R. Goto, and N. Tezuka, Japanese Journal of Applied Physics **42**, L419 (2003).
[5] K. K.-I., K. T., S. H., T. K., and T. Y., Nature **395**, 677 (1998).
[6] J.-H. Park, E. Vescovo, H.-J. Kim, C. Kwon, R. Ramesh, and T. Venkatesan, Nature **392**, 794 (1998).
[7] G. Chang, S.-Y. Xu, H. Zheng, B. Singh, C.-H. Hsu, G. Bian, N. Alidoust, I. Belopolski, D. S. Sanchez, S. Zhang, H. Lin, and M. Z. Hasan, Scientific Reports **6**, 38839 (2016).
[8] Z. Diao, M. Chapline, Y. Zheng, C. Kaiser, A. G. Roy, C. Chien, C. Shang, Y. Ding, C. Yang, D. Mauri, Q. Leng, M. Pakala, M. Oogane, and Y. Ando, Journal of Magnetism and Magnetic Materials **356**, 73 (2014); K.-I. Kobayashi, T. Kimura, Y. Tomioka, H. Sawada, K. Terakura, and Y. Tokura, Phys. Rev. B **59**, 11159 (1999); P. G. van Engen, K. H. J. Buschow, R. Jongebreur, and M. Erman, Applied Physics Letters **42**, 202 (1983), http://dx.doi.org/10.1063/1.93849; H. van Leuken and R. A. de Groot, Phys. Rev. Lett. **74**, 1171 (1995).
[9] P. W. Anderson and E. I. Blount, Physical Review Letters **14**, 217 (1965).
[10] Y. Shi, Y. Guo, X. Wang, A. J. Princep, D. Khalyavin, P. Manuel, Y. Michiue, A. Sato, K. Tsuda, S. Yu, M. Arai, Y. Shirako, M. Akaogi, N. Wang, K. Yamaura, and A. T. Boothroyd, Nature Materials **12**, 1024 (2013).
[11] S. Lei, M. Gu, D. Puggioni, G. Stone, J. Peng, J. Ge, Y. Wang, B. Wang, Y. Yuan, K. Wang, Z. Mao, J. M. Rondinelli, and V. Gopalan, Nano Letters **18**, 3088 (2018).
[12] G. Cao, S. McCall, J. E. Crow, and R. P. Guertin, Phys. Rev. Lett. **78**, 1751 (1997).
[13] D. Puggioni and J. M. Rondinelli, Nat. Commun. **5**, 3432 (2013).
[14] N. A. Benedek and T. Birol, J. Mater. Chem. C **4**, 4000 (2016).
[15] V. M. Edelstein, Phys. Rev. Lett. **75**, 2004 (1995); Phys. Rev. B **72**, 172501 (2005); D. Varjas, A. G. Grushin, R. Ilan,

and J. E. Moore, Phys. Rev. Lett. **117**, 257601 (2016).
[16] V. M. Edelstein, Journal of Physics: Condensed Matter **8**, 339 (1996); E. Bauer, H. Kaldarar, R. Lackner, H. Michor, W. Steiner, E.-W. Scheidt, A. Galatanu, F. Marabelli, T. Wazumi, K. Kumagai, and M. Feuerbacher, Phys. Rev. B **76**, 014528 (2007); E. Bauer, G. Rogl, X.-Q. Chen, R. T. Khan, H. Michor, G. Hilscher, E. Royanian, K. Kumagai, D. Z. Li, Y. Y. Li, R. Podloucky, and P. Rogl, **82**, 064511 (2010).
[17] V. P. Mineev and Y. Yoshioka, Phys. Rev. B **81**, 094525 (2010); V. M. Edelstein, Physical Review B **83**, 113109 (2011).
[18] J. P. Perdew, M. Ernzerhof, and K. Burke, J. Chem. Phys. **105**, 9982 (1996).
[19] G. Kresse and J. Furthmüller, Computational Materials Science **6**, 15 (1996).
[20] P. E. Blöchl, O. Jepsen, and O. K. Andersen, Physical Review B **49**, 16223 (1994).
[21] H. J. Monkhorst and J. D. Pack, Physical Review B **13**, 5188 (1976).
[22] S. L. Dudarev, G. A. Botton, S. Y. Savrasov, C. J. Humphreys, and A. P. Sutton, Physical Review B **57**, 1505 (1998).
[23] M. Ardit, G. Cruciani, M. Dondi, M. Merlini, and P. Bouvier, Phys. Rev. B **82**, 064109 (2010).
[24] J. Choisnet, N. Abadzhieva, P. Stefanov, D. Klissurski, J. M. Bassat, V. Rives, and L. Minchev, J. Chem. Soc., Faraday Trans. **90**, 1987 (1994).
[25] Q. Lei, M. Golalikhani, B. A. Davidson, G. Liu, D. G. Schlom, Q. Qiao, Y. Zhu, R. U. Chandrasena, W. Yang, A. X. Gray, E. Arenholz, A. K. Farrar, D. A. Tenne, M. Hu, J. Guo, R. K. Singh, and X. Xi, npj Quantum Materials **2**, 10 (2017).
[26] G. King and P. M. Woodward, J. Mater. Chem. **20**, 5785 (2010).
[27] K. H. Weyrich, Ferroelectrics **104**, 183 (1990).
[28] Y. Zhou and K. M. Rabe, Phys. Rev. B **89**, 214108 (2014).
[29] D. Orobengoa, C. Capillas, M. I. Aroyo, and J. M. Perez-Mato, Journal of Applied Crystallography **42**, 820 (2009).
[30] J. M. Perez-Mato, D. Orobengoa, and M. I. Aroyo, Acta Crystallographica Section A **66**, 558 (2010).
[31] N. Rogado, J. Li, A. Sleight, and M. Subramanian, Advanced Materials **17**, 2225 (2005).
[32] M. Zhu, Y. Lin, E. W. C. Lo, Q. Wang, Z. Zhao, and W. Xie, Applied Physics Letters **100**, 062406 (2012).
[33] J. Wang, X. Hao, Y. Xu, Z. Li, N. Zu, Z. Wu, and F. Gao, RSC Adv. **5**, 50913 (2015).
[34] J. Kanamori, Journal of Physics and Chemistry of Solids **10**, 87 (1959).
[35] J. B. Goodenough, Physical Review **100**, 564 (1955).
[36] J. B. Goodenough, Journal of Physics and Chemistry of Solids **6**, 287 (1958).
[37] S. Baidya and T. Saha-Dasgupta, Phys. Rev. B **84**, 035131 (2011).
[38] H. Das, U. V. Waghmare, T. Saha-Dasgupta, and D. D. Sarma, Phys. Rev. Lett. **100**, 186402 (2008).
[39] A. M. Glazer, Acta Crystallographica Section A **31**, 756 (1975).
[40] J. Young, A. Stroppa, S. Picozzi, and J. M. Rondinelli, Journal of Physics: Condensed Matter **27**, 283202 (2015).
[41] J. Young, P. Lalkiya, and J. M. Rondinelli, J. Mater. Chem. C **4**, 4016 (2016).
[42] J. Young and J. M. Rondinelli, Phys. Rev. B **89**, 174110 (2014).
[43] N. A. Benedek and C. J. Fennie, Physical Review Letters **106**, 107204 (2011).
[44] Supporting Information at `http://supporting/xxxx`.
[45] K.-W. Lee and W. E. Pickett, Phys. Rev. B **83**, 180406 (2011).
[46] B. L. Chamberland and W. H. Cloud, Journal of Applied Physics **40**, 434 (1969).
[47] O. Bengone, M. Alouani, P. Blöchl, and J. Hugel, Phys. Rev. B **62**, 16392 (2000); A. G. Petukhov, I. I. Mazin, L. Chioncel, and A. I. Lichtenstein, Phys. Rev. B **67**, 153106 (2003).
[48] K.-W. Lee and W. E. Pickett, Phys. Rev. B **80**, 125133 (2009); M. A. Korotin, V. I. Anisimov, D. I. Khomskii, and G. A. Sawatzky, Phys. Rev. Lett. **80**, 4305 (1998).
[49] H. Raebiger, S. Lany, and A. Zunger, Nature **453**, 763 (2008).
[50] Y. Ohnuma, M. Matsuo, and S. Maekawa, Phys. Rev. B **94**, 184405 (2016).
[51] R. D. King-Smith and D. Vanderbilt, Physical Review B **47**, R1651 (1993).
[52] C.-G. Duan, C.-W. Nan, S. S. Jaswal, and E. Y. Tsymbal, Phys. Rev. B **79**, 140403 (2009).
[53] F.-R. Fan, H. Wu, D. Nabok, S. Hu, W. Ren, C. Draxl, and A. Stroppa, J. Amer. Chem. Soc. **139**, 12883 (2017).
[54] R. Wakatsuki, Y. Saito, S. Hoshino, Y. M. Itahashi, T. Ideue, M. Ezawa, Y. Iwasa, and N. Nagaosa, Science Advances **3** (2017), 10.1126/sciadv.1602390.